nature nanotechnology

ARTICLES

PUBLISHED ONLINE: 17 NOVEMBER 2013 | DOI: 10.1038/NNANO.2013.240

Detecting the translocation of DNA through a nanopore using graphene nanoribbons

F. Traversi[1], C. Raillon[1], S. M. Benameur[2], K. Liu[1], S. Khlybov[1], M. Tosun[2], D. Krasnozhon[2], A. Kis[2] and A. Radenovic[1]*

Solid-state nanopores can act as single-molecule sensors and could potentially be used to rapidly sequence DNA molecules. However, nanopores are typically fabricated in insulating membranes that are as thick as 15 bases, which makes it difficult for the devices to read individual bases. Graphene is only 0.335 nm thick (equivalent to the spacing between two bases in a DNA chain) and could therefore provide a suitable membrane for sequencing applications. Here, we show that a solid-state nanopore can be integrated with a graphene nanoribbon transistor to create a sensor for DNA translocation. As DNA molecules move through the pore, the device can simultaneously measure drops in ionic current and changes in local voltage in the transistor, which can both be used to detect the molecules. We examine the correlation between these two signals and use the ionic current measurements as a real-time control of the graphene-based sensing device.

Solid-state nanopores[1] can be used to sense[2–8] and manipulate[9,10] DNA molecules by threading the molecules through the pore under an applied potential and monitoring the ionic current passing through the pore. Although the size of the pore can be tuned[11] and the devices can be integrated with other single-molecule techniques[9,10,12] and detection mechanisms[13–16], they have yet to deliver sequencing data. One reason for this is that the nanopores are typically fabricated in SiN_x or SiO_2 membranes, which have thicknesses that are large compared to the size of a DNA base. Graphene[17] nanopores have recently been used as an alternative to traditional solid-state nanopores[18–20]. In these devices, graphene acts as the membrane material, which allows, in principle, single-base resolution in the ionic current due to its single-atom thickness. However, the relatively large dimensions of the graphene layer in this proposed geometry mean it cannot be used as a sensing electrode, and the reliance on ionic current measurements precludes multiplexing.

A complementary approach is to integrate the standard, relatively thick SiN_x membrane with a sensing electrode. A variety of sensing electrodes have been theoretically proposed for this purpose, including metallic tunnelling electrodes[21], graphene nanogaps[22] and graphene nanoribbons (GNRs)[23]. The detection of single translocation events has also been demonstrated experimentally using metallic nanogaps and electrical tunnelling measurements[24]. Although tunnelling detection could in principle be used to achieve single base resolution, the alignment of the active tunnelling area with the nanopore remains a significant issue. Alternatively, silicon nanowire field-effect transistors have previously been combined with a solid-state nanopore to detect DNA translocation[16].

Nanopore with a GNR device

To fabricate our devices (Fig. 1) we began by creating a 20-nm-thick SiN_x membrane (~20 μm × 20 μm in size), followed by the transfer of a chemical vapour deposition (CVD)-grown graphene monolayer (Fig. 2b,e). Graphene nanoribbons were defined using electron-beam lithography (EBL) and oxygen reactive ion etching (RIE). Next, electrical contacts were fabricated by EBL, electron-beam evaporation of a Cr (5 nm)/Au (50 nm) metal double layer and lift-off (Fig. 2c,f). To minimize the ionic cross-conductance we carried out atomic layer deposition (ALD) of 5 nm Al_2O_3, which was expected to isolate the electrodes from the electrolyte solution[16]. Finally, nanopore drilling was performed in a transmission electron microscope (TEM) working in scanning mode[25], as shown in Fig. 2d,h (for more details see 'Device fabrication' section of the Methods). The resulting structure is a GNR defined on the SiN_x membrane with a nanopore located in its centre.

To perform device characterization and experiments, we placed our chips in a custom-made microfluidic chamber (Fig. 1c) in order to carry out simultaneous measurements of the current flowing through the GNR and the ionic current flowing through the nanopore (for more details see 'Experimental set-up' section of the Methods). We performed our experiments in three different solutions: buffered 1 M KCl (10 mM Tris, 1 mM EDTA, pH 7.4), buffered 10 mM KCl (10 mM Tris, 1 mM EDTA, pH 7.4) and salt gradient conditions (10 mM KCl in the *cis* chamber, 100 mM KCl, 10 mM Tris, 1 mM EDTA, pH 7.4 in the *trans* chamber). The current–voltage (I–V) characteristics of the nanopores and GNRs were acquired before the translocation experiments. To evaluate the influence of the presence of the GNR on the ionic I–V characteristics of the nanopore, we first characterized the pore with the GNR disconnected from the instrumentation. We then connected the GNR and repeated the ionic current measurement. We proceeded with measurements only using pores showing linear I–V characteristics in both cases, which indicated that the integration of the GNR with the pore had not resulted in rectifying behaviour. In Fig. 1e we show a typical nanopore I–V characteristic in 10 mM KCl with the GNR connected to the instrumentation. The total noise level usually increased considerably when connecting the GNR to the instrumentation, from typically 40 pA (root mean square, r.m.s.) to 100 pA r.m.s. in 10 mM KCl (Supplementary Fig. 5). In the next characterization step, we measured the resistance of the GNR. Figure 1f presents measurements performed on a GNR (with a resistance of 122 kΩ) obtained in a 10 mM KCl solution. The resistance of the same GNR in air was

[1]Laboratory of Nanoscale Biology, Institute of Bioengineering, School of Engineering, EPFL, 1015 Lausanne, Switzerland, [2]Laboratory of Nanoscale Electronics and Structure, Institute of Electrical Engineering, School of Engineering, EPFL, 1015 Lausanne, Switzerland. *e-mail: aleksandra.radenovic@epfl.ch

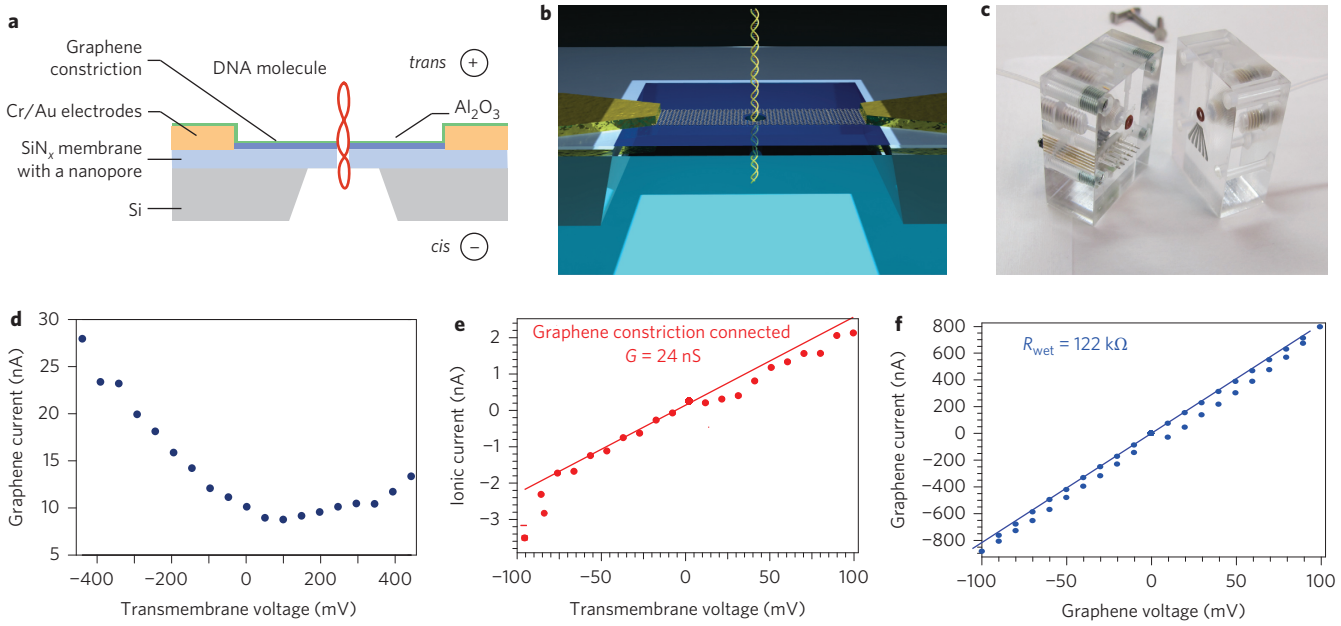

Figure 1 | Schematics and characterization of the GNR transistor–nanopore measuring set-up. a, Schematic of the set-up (side view). A single DNA molecule is translocating through a nanopore fabricated in a SiN_x membrane. **b**, Artistic representation of the device. **c**, Photograph of the fluidic cell. **d**, I–V_G characteristics of a liquid-gated GNR with a nanopore in 10 mM KCl. Gating is performed by changing the transmembrane voltage while $V_{sd} = 5$ mV. **e**, I–V characteristic of a 10 nm nanopore in 10 mM KCl buffer after connecting the GNR. Dots are experimental points, and the continuous line is the fit from which the value of the conductance is extrapolated. **f**, I–V characteristic of a GNR in 10 mM KCl (same device as in **e**). Dots are experimental points, and the continuous line is the fit from which the value of the resistance is extrapolated. R_{wet} means in buffer conditions as opposed to dry conditions.

275 kΩ. We attribute this decrease in resistance to doping due to the high ionic strength of our solution[26]. To exclude the possibility of leakage through the ionic solution and to verify the quality of the passivation layer, we analysed the ionic current measured as a function of the ionic bias in samples without a drilled pore (Supplementary Fig. 6). This allowed us to quantify the current (measured by an Axopatch patch clamp amplifier) originating from sources other than the pore, that is, the current leaking from the graphene. In the measurement displayed in Supplementary Fig. 6, V_p was swept from −400 mV to 400 mV, a range that corresponds to the range used in translocation experiments. A maximum current of 20 pA was measured for $V_p = 400$ mV, setting a minimum value for the oxide resistance (R_{oxide} of Fig. 5 and Supplementary Fig. 7) of more than 10 GΩ. This means that the Al_2O_3 passivation layer on the GNRs and the electrodes isolates the GNR device from the solution. To exclude the possibility of leakage through the ionic solution in devices with a pore (the ones used in the experiments) and to verify the quality of the passivation layer, we performed a resistance measurement between two control electrodes placed in the vicinity of the GNR. In most samples we obtained resistances in the range of 1–10 GΩ, consistent with the results in Supplementary Fig. 6. Devices with resistance lower than 100 MΩ measured between disconnected electrodes were discarded at this point. We finally added DNA into the *cis* chamber. For translocation experiments, a bias voltage in the 100–400 mV range was applied to the Ag/AgCl electrodes with the bias voltage across the GNR set to 20–100 mV. After some time, we began to observe events (Fig. 3a). The applied bias was always positive for devices with the graphene transistor placed on the *trans* side of the membrane. A gallery of typical events is shown in Supplementary Fig. 4. In our experiments, the passage of the molecule through the pore results in a drop in ionic current. This is considered usual in SiN_x at high ionic strengths (1 M KCl), although for lower salt concentrations current increases are expected[27,28]. The pores used in our experiments were drilled in a SiN_x membrane onto which a layer of Al_2O_3 had been deposited. The presence of the thin alumina layer on the walls of the pore changes the surface charge from negative to positive, allowing current drops to be negative even at very low ionic strengths (10 mM KCl)[29,30]. Interestingly, we observed both dips and spikes in the electrical current flowing through the GNR. This behaviour is compatible with the ambipolar nature of graphene.

DNA detection through a nanopore using GNRs

In experiments using a 10 mM KCl buffer, we translocated circular plasmid pNEB, a 2,713-bp-long derivative of the pUC19 plasmid. The initial concentration in the *cis* chamber was 28 μM. Figure 3a shows part of the signal acquired in these experimental conditions. A total of 125 ionic events were detected and analysed in this experiment, 70 of which show correlations with changes in the graphene current. Figure 3b presents a magnified view of a single correlated event, an event where the translocation of the DNA molecule has generated a drop in the ionic current, together with a change in the graphene current. In this particular data set, events correspond to spikes in the graphene current. Other experimental runs, performed in 10 mM and 1 M KCl buffer solutions, can also show current dips (for details see Supplementary Fig. 3).

Translocation events in the ionic and graphene current were detected using custom event detection and classification software written in MATLAB. Event detection was run separately for the ionic current and the graphene current data, and events were identified by an abrupt change detection algorithm[31,32]. The dwell times and current drops were computed automatically and are represented in the scatter plots shown in Fig. 3c and d for ionic current and graphene current, respectively. A correlation analysis was then performed on the two event sets. To isolate the subset of correlated events, a cut-off delay time of 3 ms was chosen. This interval is arbitrary and was chosen to ensure the identification of all correlated events. A quantitative time delay analysis showed that all of the

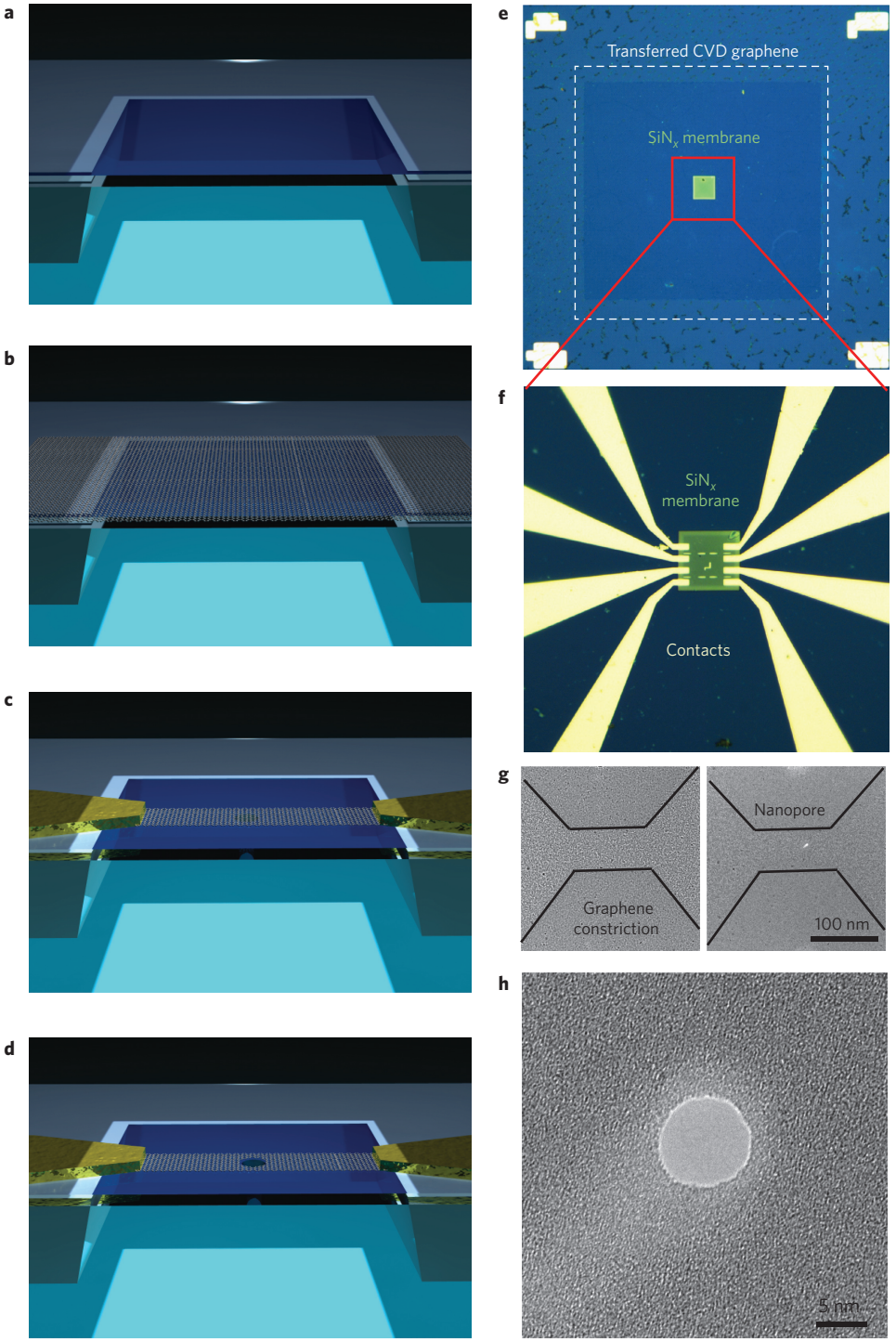

Figure 2 | Fabrication of a solid-state nanopore with a GNR transistor. a–d, Schematics of device fabrication steps: fabrication of SiN_x membrane (**a**); transfer of CVD graphene monolayer (**b**); graphene nanoribbon pattering and electrode fabrication (**c**); pore drilling (**d**). **e**, Optical micrograph of a SiN_x membrane with a transferred CVD graphene monolayer on top. The dashed line highlights the transferred CVD graphene monolayer. Image dimensions, 250 μm × 250 μm. **f**, Optical micrograph of Cr/Au electrodes contacting four GNRs on the SiN_x membrane. From four GNRs we select one for drilling. Image dimensions, 120 μm × 120 μm. **g**, TEM micrographs of a GNR before (left) and after (right) drilling. **h**, TEM image of a nanopore (same device as in Fig. 1e).

events considered as correlated have an actual delay time lower than 250 μs. We can isolate two types of events in the scatter plot of the events detected in the ionic current. One cluster of events has dwell times of between 200 μs and 2 ms and current drops between 0.3 nA and 0.5 nA. The second event cluster has dwell times between 40 μs and 200 μs and current drops between 0.1 nA and 0.5 nA. Most of the events belonging to the first cluster (there are only five exceptions in the discussed experiment) are correlated with an event detected in the graphene current. In contrast, almost no events belonging to the second cluster are correlated with events detected in the graphene current. We find two similar clusters in the scatter plot of the events detected in the graphene current. We can identify a cluster of mostly correlated events with dwell times between 200 μs and 3 ms and current increases

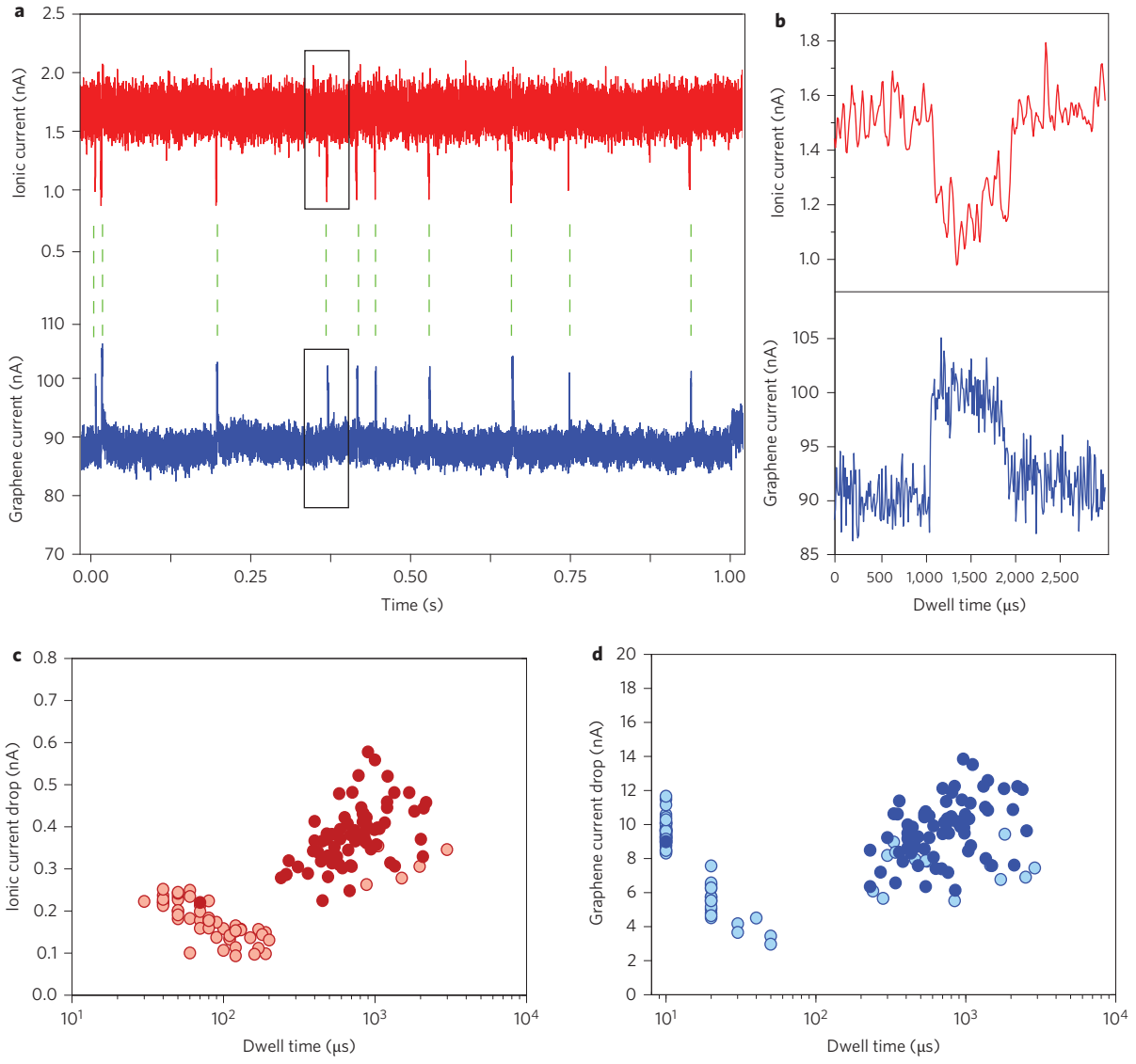

Figure 3 | Simultaneous detection of DNA translocations in ionic and graphene current. a, Simultaneously recorded ionic current and electrical current flowing through the GNR during translocations of pNEB DNA in 10 mM KCl (transmembrane voltage, 200 mV; graphene source–drain voltage, 20 mV). Ionic current is displayed in red and graphene current in blue. Green lines indicate the position of the correlated events in the ionic and graphene current. **b**, Zoom-in view of a single correlated event. **c**, Scatter plot of the events detected in the ionic current. **d**, Scatter plot of the events detected in the graphene current. Correlated events are represented by filled coloured circles, and uncorrelated events by partially transparent circles.

between 5 nA and 10 nA. The uncorrelated events have much shorter dwell times (less than 50 μs).

Under our experimental conditions, with a SiN_x thickness of ~20 nm and electric field strength inside the nanopore reaching 1×10^6 V m^{-1}, one can assume that the segment of the dsDNA with a persistence length of 50 nm translocates the pore in a fully extended form[33]. Although we used circular DNA plasmid in the supercoiled form, we assume that the supercoiled DNA form is (at least in the pore region) locally underwound, meaning that two dsDNA molecules are translocating the pore at the same time, fully extended. We attribute the correlated events detected in both channels to this type of translocation. Events in the graphene current can be explained by the model proposed in a recent work by Xie and colleagues[16]. In their publication they propose a DNA sensing device similar to the one presented in this Article, but a p-doped silicon nanowire field-effect transistor (FET) was used to sense the translocation of the DNA molecules[16]. Their proposed sensing mechanism does not rely on a direct interaction between the DNA and the sensor. Instead, the FET senses changes in the local electric potential in the proximity of the pore. In our case, this type of gating is compatible with both types of event because of the ambipolar nature of the charge carriers in single-layer graphene. In Fig. 1d we show the characterization of the conductivity of the GNR as a function of the voltage applied across the pore. Because the GNR is located in the *trans* chamber, the positive ionic electrode acts as the gate for the graphene device[34]. In the data presented here, the graphene current shows a minimum close to 0 V, corresponding to the Dirac point in graphene (V_D). For voltages lower than V_D, current is carried by holes and the material has p-type behaviour, whereas for higher voltages the current is carried by electrons and the material shows n-type behaviour. Device-to-device variability can result in devices operating in one of these regimes for positive voltages between 100 mV and 400 mV, values that are required to obtain DNA translocations through the pore. A change in the electric field near the pore due to the presence of the DNA molecule would generate current increases in the graphene current when operating the device in the p-type regime and current decreases for n-type devices. Our results are quantitatively

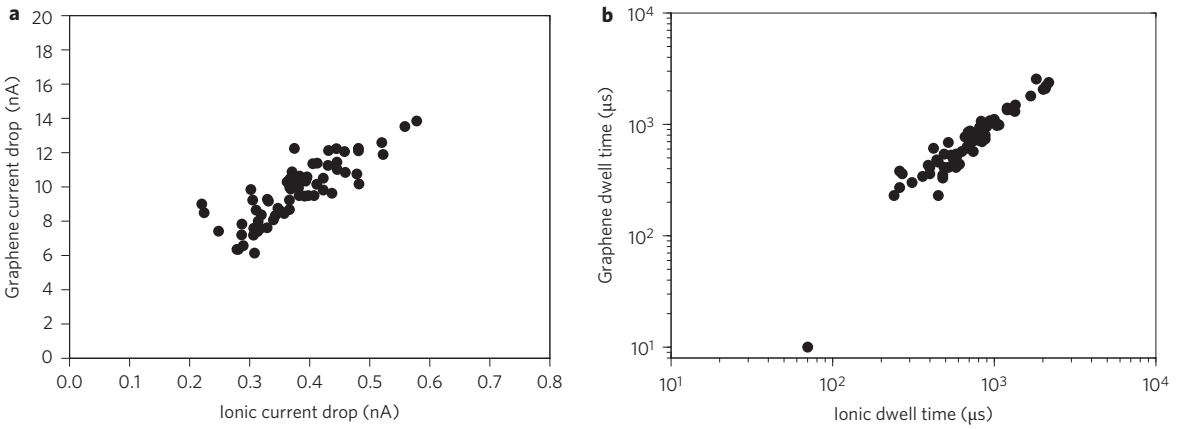

Figure 4 | Event correlation graphs display events detected both in ionic and graphene current. a,b, Event correlation graph of the amplitudes (**a**) and dwell times (**b**) of correlated events displayed in Fig. 3a,b.

consistent with the results of the simulation in ref. 16. Specifically, Fig. 3 shows increases in the graphene current of the order of 10%. This is compatible with a change in the gating potential of the order of 20 mV, as shown in Fig. 1d. To better understand the magnitude of the potential change due to the presence of DNA, we performed numerical simulations (detailed in the Supplementary Fig. 4 and shown in Supplementary Fig. 12c). To simplify the estimation of the electric potential change due to the presence of DNA in the nanopore under our experimental conditions, we adopted the approach proposed by van Dorp and colleagues[33] and assumed an additive contribution from the two DNA segments. We found that one 50-nm-long linear dsDNA segment attenuates the potential at the position of the graphene device for 8 mV (Supplementary Fig. 12), resulting in a potential change of $\Delta V = 16$ mV due to translocation of the complete DNA plasmid.

Because both the pore current and the change in electrostatic potential in the proximity of the pore are proportional to the effective cross-sectional area of the DNA present in the pore, one should expect a correlation between the amplitudes of ionic and graphene events. Event correlation graphs of current drops and dwell times of correlated events are shown in Fig. 4a and b, respectively. In both cases, the observed relationship between the two quantities is almost linear; that is, long and deep events in the ionic current are correlated to long and large increases in the graphene current.

Non-correlated events, characterized by fast and shallow dips in the ionic current, could be attributed to DNA molecules bumping against the pore instead of translocating through it[35]. During such bumping events, the clogging of the pore is too weak to effectively change the electrostatic potential in the proximities of the pore and gate the GNR. Very fast events detected in the graphene current but not visible in the ionic current could be attributed to local changes in the electrical conductivity of the GNR due to the presence of charged molecules in the solution far from the pore.

An electrical model of the entire device has been developed in Advanced Design Systems (ADS, Agilent Technologies). The full model is shown in Supplementary Fig. 7, and the equivalent circuit is presented in Fig. 5 together with the circuit adapted from ref. 16. The key block of the model is the parallel circuit composed of the resistance and the capacitance associated with the aluminium oxide deposited on the graphene (R_{oxide} and C_{oxide} respectively). R_{oxide}, in particular, needs to be as high as possible (in our case 10 GΩ) to ensure a good isolation of the graphene constriction from the electrolyte. The values of the various lumped elements governing the model for both ionic strengths of electrolyte are listed in Supplementary Table 1. To exclude crosstalk as a possible cause for the changes in the graphene current we performed simulations as detailed in Supplementary Fig. 7. We found that simulated sudden changes in ionic current did not result in changes in the graphene current, leaving electrostatic gating as the only physical reason for the current drops (or increases) in I_g (Supplementary Fig. 8).

Conclusions

Our experiments show a relatively low translocation rate, which can be attributed to several factors such as low analyte concentration, low transmembrane voltage, potential distribution around the pore (Supplementary Fig. 11) and restricted options for nanopore cleaning and storage treatments. To increase the translocation rate, we adopted two published strategies. We operated the device under gradient conditions (as suggested by Wanunu *et al.*[36]) and increased the transmembrane voltage bias from 200 mV to 400 mV. To preserve the quality of the Al_2O_3 passivation layer, we maintained a low ionic strength of 10 mM on the membrane side housing the GNR device, now on the *cis* side, as illustrated in the

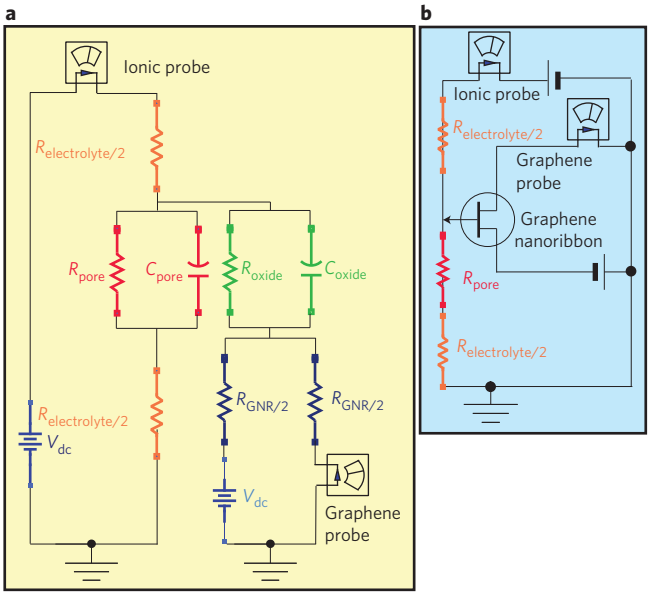

Figure 5 | Equivalent circuit diagrams for a GNR nanopore device. **a**, Circuit diagram of device. **b**, Circuit diagram used for the crosstalk analysis performed in ADS software (Supplementary Figs 7 and 8). The effects of gating have been neglected and GNR is modelled with resistors. The passivation layer is represented by a parallel resistor (R_{oxide}) and capacitance (C_{oxide}).

schematics in Supplementary Fig. 10. Note that these gradient conditions are opposite to the gradient conditions presented in the work by Xie *et al.*[16], where the ionic strength gradient is used not to increase the capture rate but to enhance the changes in the local electric potential in the proximity of the pore. Indeed, in this condition we obtained a fourfold increase in the translocation rate. In the same time, application of the higher transmembrane potential increased the current blockage amplitude and decreased the average translocation time, as shown in Supplementary Fig. 10c,d, respectively. We observed 923 events in the graphene channel (41% correlated) and 532 events in the ionic channel (71% correlated), with average amplitudes of 5 nA and 1 nA, respectively. Although we achieved a lower translocation rate at 200 mV transmembrane bias, the DNA translocation time was longer, facilitating event analysis. We have demonstrated the operation of a novel device based on the integration of a GNR with a solid-state SiN_x nanopore. The device was used to detect the translocation of pNEB DNA and λ-DNA molecules through a solid-state nanopore drilled in graphene and thin SiN_x membrane. Experiments were carried out at different ionic strengths between 10 mM KCl and 1 M KCl, showing that the device can operate in a broad range of ionic strength conditions. Ionic current and graphene current were recorded simultaneously, and translocation events were detected in both channels. Events show clear correlation with the translocation events detected in the ionic pore current. This is the first time that translocation events of single DNA molecules have been detected by electrical means other than the ionic current itself, using a graphene-based device integrated on a solid-state nanopore. The use of a two-dimensional material, such as graphene, in the sensor device opens up the possibility of increasing the resolution of solid-state nanopore-based devices and the integration of more than one detector per chip. Moreover, graphene is not the only suitable material for this kind of sensor. Other two-dimensional materials, such as the recently investigated MoS_2 (refs 37,38), with semiconducting properties and a stronger field effect with respect to graphene are particularly interesting from this point of view.

Methods

Device fabrication. We prepared our samples starting from boron-doped 380-μm-thick silicon chips. Chips were coated on both sides with a 60-nm-thick layer of SiO_2 and a 20 nm top layer of low-stress SiN_x. The thickness of the SiN_x was chosen for structural reasons, and the thickness of the SiO_2 was chosen to optimize the visibility of the grapheme, enhancing the optical contrast with the bare substrate[39] (Supplementary Fig. 1a). A square window (~500 μm × 500 μm) was opened in the SiO_2/SiN_x layer on the back side by EBL and RIE. Chips were then wet etched in KOH to remove the silicon and the frontside SiO_2 layer, resulting in a square SiN_x membrane (~20 μm × 20 μm, Fig. 2a). Large-area graphene films were grown on copper foils[40]. The growth took place under the flow of a methane/argon/hydrogen reaction gas mixture at a temperature of 1,000 °C. At the end of the growth, the temperature was decreased rapidly and the gas flow turned off. The copper foils were then coated with poly(methylmethacrylate) (PMMA) and the copper etched away, resulting in a centimetre-scale graphene film ready to be transferred onto the chips with membranes (Fig. 2b,e). This graphene was single layer, continuous and had good electronic properties. We measured a room-temperature mobility on SiO_2 of $\mu = 2{,}700\ cm^2\ V^{-1}\ s^{-1}$ (Supplementary Fig. 1b). Before depositing graphene on the chip, the substrate was prepatterned using EBL, opening an ~200 μm × 200 μm square in a methyl methacrylate (MMA)/PMMA electron-beam resist double layer. A subsequent liftoff process was used to remove the graphene layer everywhere but on the opening, that is, the region over and around the membrane, as shown in Fig. 2b[41]. GNRs were then patterned by EBL and oxygen RIE and contacted by EBL, followed by evaporation of a Cr 5 nm/Au 50 nm metal double layer and liftoff (Fig. 2c,f). Chips were then cleaved to a size of 8 mm × 4 mm to fit the TEM holder. A 15-min-long immersion in *N*-methyl-2-pyrrolidone (NMP) at 75 °C was carried out before Al_2O_3 ALD deposition in order to functionalize the graphene surface and allow uniform adhesion of the thin oxide layer on it. ALD was performed by cyclically pumping trimethyl aluminium (TMA) and water vapour (H_2O) at a temperature of 200 °C. Precursors were diluted in a constant N_2 flux at a base pressure of 60 mbar. Al_2O_3 was typically deposited up to a thickness of 5 nm before pore drilling.

Electron beam drilling[25] was performed using a Philips JEOL 2200FS TEM. We found drilling in the STEM mode to be more suitable for our purposes. We operated the microscope at an acceleration voltage of 200 kV. Before being loaded into the microscope, the samples were cleaned at 400 °C under H_2/Ar flux to remove any residual organic material left on the surface by the microfabrication process. Samples were first imaged in TEM mode to identify the GNR with the best characteristics. Nanoribbons with a width of ~100 nm and well-defined edges were usually chosen for drilling (smaller nanoribbons are usually very highly resistive after drilling). After imaging, the microscope operating mode was switched to STEM. A mechanical stabilization period of at least 30 min was mandatory to avoid drifting of the sample during drilling and to drill round pores. A 2 nm beam in analytical magnification mode was chosen for drilling. To minimize the sample exposure time at the highly energetic beam, only a very fast (low resolution) image was taken in STEM mode. The raster scan was then stopped, and the beam blanked and driven via software to the place where the hole was to be drilled. We observed a typical drilling time of 3 min for a 20 nm, low-stress SiN_x membrane, with graphene and 5 nm of Al_2O_3 on top. The opening of the pore could be monitored in real time by recording the changes occurring in the Ronchigram displayed on the fluorescent screen. This allowed the user to stop the drilling as soon as the pore was open, avoiding additional exposure of the GNR to the electron beam. A TEM image of a GNR before and after drilling is shown in Fig. 2g, and a magnified image of a typical pore is shown in Fig. 2h. Properties of working devices are listed in Supplementary Table 2.

Experimental set-up. The chip was sealed by silicone o-rings between two PMMA chambers that work as reservoirs. The microfluidics support was equipped with six metallic connectors, connected to the instrumentation through a set of pins and cables. Ohmic contact between the metallic connectors on the microfluidics support and the device was obtained using drops of silver paste deposited on the gold pads on the chip. No particular chemical cleaning was performed on these nanopores. Standard wetting treatments like cleaning in piranha solution or soft O_2 plasma cleaning were not applicable on our samples because they would remove graphene. This could account for the observed low DNA molecule capture rate. After mounting the sample in the microfluidic set-up, the wetting of the pore was promoted by flushing with 50% water–50% ethanol solution for 8–12 h.

We used a FEMTO 400 kHz current amplifier to preamplify the graphene current and an Axopatch 200B patch clamp amplifier (100 kHz acquisition rate, 10 kHz Bessel filter) for the ionic current. We used an NI PXI-4461 card for data digitalization and custom-made LabView software for data acquisition. We found a good signal-to-noise ratio by filtering at 10 kHz and sampling at 100 kHz. Chlorinated Ag/AgCl electrodes were inserted into both reservoirs and connected to the Axopatch 200B.

COMSOL modelling. Finite-element simulations of the electric potential distributions were performed using COMSOL Multiphysics v. 4.2. To simulate our experimental situation, we used the full Nernst–Planck equations for the ionic concentrations and Poisson's equation for the electrostatic potential. The system was analysed in the steady state by placing each chamber in contact with a bath maintained at specified concentrations and under different surface charge conditions (zero, $-8\ mC\ m^{-2}$ and $50\ mC\ m^{-2}$). Translocating and trapped DNA were modelled as previously described[33,42].

Received 31 October 2012; accepted 14 October 2013; published online 17 November 2013

References

1. Li, J. *et al.* Ion-beam sculpting at nanometre length scales. *Nature* **412,** 166–169 (2001).
2. Li, J. L., Gershow, M., Stein, D., Brandin, E. & Golovchenko, J. A. DNA molecules and configurations in a solid-state nanopore microscope. *Nature Mater.* **2,** 611–615 (2003).
3. Fologea, D. *et al.* Detecting single stranded DNA with a solid state nanopore. *Nano Lett.* **5,** 1905–1909 (2005).
4. Storm, A. J., Chen, J. H., Zandbergen, H. W. & Dekker, C. Translocation of double-strand DNA through a silicon oxide nanopore. *Phys. Rev. E* **71,** 051903 (2005).
5. Dekker, C. *et al.* Salt dependence of ion transport and DNA translocation through solid-state nanopores. *Nano Lett.* **6,** 89–95 (2006).
6. Skinner, G. M., van den Hout, M., Broekmans, O., Dekker, C. & Dekker, N. H. Distinguishing single- and double-stranded nucleic acid molecules using solid-state nanopores. *Nano Lett.* **9,** 2953–2960 (2009).
7. Van den Hout, M., Krudde, V., Janssen, X. J. A. & Dekker, N. H. Distinguishable populations report on the interactions of single DNA molecules with solid-state nanopores. *Biophys. J.* **99,** 3840–3848 (2010).
8. Wanunu, M. *et al.* Rapid electronic detection of probe-specific microRNAs using thin nanopore sensors. *Nature Nanotech.* **5,** 807–814 (2010).
9. Keyser, U. F. *et al.* Direct force measurements on DNA in a solid-state nanopore. *Nature Phys.* **2,** 473–477 (2006).
10. Trepagnier, E. H., Radenovic, A., Sivak, D., Geissler, P. & Liphardt, J. Controlling DNA capture and propagation through artificial nanopores. *Nano Lett.* **7,** 2824–2830 (2007).
11. Dekker, C. Solid-state nanopores. *Nature Nanotech.* **2,** 209–215 (2007).

12. Peng, H. B. & Ling, X. S. S. Reverse DNA translocation through a solid-state nanopore by magnetic tweezers. *Nanotechnology* **20,** 185101 (2009).
13. Taniguchi, M., Tsutsui, M., Yokota, K. & Kawai, T. Fabrication of the gating nanopore device. *Appl. Phys. Lett.* **95,** 123701 (2009).
14. McNally, B. *et al.* Optical recognition of converted DNA nucleotides for single-molecule DNA sequencing using nanopore arrays. *Nano Lett.* **10,** 2237–2244 (2010).
15. Tsutsui, M. *et al.* Single-molecule sensing electrode embedded in-plane nanopore. *Sci. Rep.* **1,** 46 (2011).
16. Xie, P., Xiong, Q. H., Fang, Y., Qing, Q. & Lieber, C. M. Local electrical potential detection of DNA by nanowire–nanopore sensors. *Nature Nanotech.* **7,** 119–125 (2012).
17. Geim, A. K. Graphene: status and prospects. *Science* **324,** 1530–1534 (2009).
18. Garaj, S. *et al.* Graphene as a subnanometre trans-electrode membrane. *Nature* **467,** 190–193 (2010).
19. Merchant, C. A. *et al.* DNA translocation through graphene nanopores. *Nano Lett.* **10,** 2915–2921 (2010).
20. Schneider, G. F. *et al.* DNA translocation through graphene nanopores. *Nano Lett.* **10,** 3163–3167 (2010).
21. Lagerqvist, J., Zwolak, M. & Di Ventra, M. Fast DNA sequencing via transverse electronic transport. *Nano Lett.* **6,** 779–782 (2006).
22. Postma, H. W. Rapid sequencing of individual DNA molecules in graphene nanogaps. *Nano Lett.* **10,** 420–425 (2010).
23. Min, S. K., Kim, W. Y., Cho, Y. & Kim, K. S. Fast DNA sequencing with a graphene-based nanochannel device. *Nature Nanotech.* **6,** 162–165 (2011).
24. Ivanov, A. P. *et al.* DNA tunneling detector embedded in a nanopore. *Nano Lett.* **11,** 279–285 (2011).
25. Storm, A. J., Chen, J. H., Ling, X. S., Zandbergen, H. W. & Dekker, C. Fabrication of solid-state nanopores with single-nanometre precision. *Nature Mater.* **2,** 537–540 (2003).
26. Ang, P. K., Chen, W., Wee, A. T. S. & Loh, K. P. Solution-gated epitaxial graphene as pH sensor. *J. Am. Chem. Soc.* **130,** 14392–14393 (2008).
27. Smeets, R. M. M., Dekker, N. H. & Dekker, C. Low-frequency noise in solid-state nanopores. *Nanotechnology* **20,** 095501 (2009).
28. Kuan, A. T. & Golovchenko, J. A. Nanometer-thin solid-state nanopores by cold ion beam sculpting. *Appl. Phys. Lett.* **100,** 213104 (2012).
29. Dimitrov, V. *et al.* Nanopores in solid-state membranes engineered for single molecule detection. *Nanotechnology* **21,** 065502 (2010).
30. Venkatesan, B. M., Shah, A. B., Zuo, J. M. & Bashir, R. DNA sensing using nanocrystalline surface-enhanced Al_2O_3 nanopore sensors. *Adv. Funct. Mater.* **20,** 1266–1275 (2010).
31. Raillon, C. *et al.* Nanopore detection of single molecule RNAP–DNA transcription complex. *Nano Lett.* **12,** 1157–1164 (2012).
32. Raillon, C., Granjon, P., Graf, M., Steinbock, L. J. & Radenovic, A. Fast and automatic processing of multi-level events in nanopore translocation experiments. *Nanoscale* **4,** 4916–4924 (2012).
33. Van Dorp, S., Keyser, U. F., Dekker, N. H., Dekker, C. & Lemay, S. G. Origin of the electrophoretic force on DNA in solid-state nanopores. *Nature Phys.* **5,** 347–351 (2009).
34. Heller, I. *et al.* Comparing the weak and strong gate-coupling regimes for nanotube and graphene transistors. *Phys. Status Solidi* **3,** 190–192 (2009).
35. Harrell, C. C. *et al.* Resistive-pulse DNA detection with a conical nanopore sensor. *Langmuir* **22,** 10837–10843 (2006).
36. Wanunu, M., Morrison, W., Rabin, Y., Grosberg, A. Y. & Meller, A. Electrostatic focusing of unlabelled DNA into nanoscale pores using a salt gradient. *Nature Nanotech.* **5,** 160–165 (2010).
37. Novoselov, K. S. *et al.* Two-dimensional atomic crystals. *Proc. Natl Acad. Sci. USA* **102,** 10451–10453 (2005).
38. Radisavljevic, B., Radenovic, A., Brivio, J., Giacometti, V. & Kis, A. Single-layer MoS_2 transistors. *Nature Nanotech.* **6,** 147–150 (2011).
39. Blake, P. *et al.* Making graphene visible. *Appl. Phys. Lett.* **91,** 063124 (2007).
40. Li, X. S. *et al.* Large-area synthesis of high-quality and uniform graphene films on copper foils. *Science* **324,** 1312–1314 (2009).
41. Ye, Y. *et al.* A simple and scalable graphene patterning method and its application in CdSe nanobelt/graphene Schottky junction solar cells. *Nanoscale* **3,** 1477–1481 (2011).
42. Vlassarev, D. M. & Golovchenko, J. A. Trapping DNA near a solid-state nanopore. *Biophys. J.* **103,** 352–356 (2012).

Acknowledgements

This work was supported financially by the European Research Council (grant no. 259398, PorABEL: Nanopore Integrated Nanoelectrodes for Biomolecular Manipulation and Sensing). F.T. was partially financed by an FP7 nanoDNA sequencing grant. C.R. was financed by a grant from the Swiss SystemsX.ch initiative (IPhD), evaluated by the Swiss National Science Foundation. M.B. and D.K. were supported by grants from the Swiss National Science Foundation (grants nos 122044 and 135046). The authors thank the Centre Interdisciplinaire de Microscopie Electronique (CIME) at EPFL for access to electron microscopes, and special thanks go to D.T.L. Alexander for providing training and technical assistance with TEM. Device fabrication was partially carried out at the EPFL Center for Micro/Nanotechnology (CMi). The authors thank A. Ionescu and Nanolab (EPFL) for access to Advance Design System (ADS) software and A. Bazigos for help with ADS. Thanks go to V. Russo and C.S. Casari of the Politecnico di Milano for Raman spectroscopy on graphene, P. Granjon (Grenoble Institute of Technology) for help with the crosstalk analysis, and all LBEN laboratory members for reviewing the manuscript.

Author contributions

F.T., A.K. and A.R. designed the research. F.T. and A.R. designed and built the measurement set-up. F.T. fabricated and characterized devices, performed experiments and analysed the data. K.L. performed experiments and analysed the data. C.R. and M.B. worked on the first generation of devices based on exfoliated graphene. S.K. performed COMSOL modelling. M.T. and D.K. performed CVD graphene growth and transfer. F.T., A.K. and A.R. wrote the paper.

Additional information

Supplementary information is available in the online version of the paper. Reprints and permissions information is available online at www.nature.com/reprints. Correspondence and requests for materials should be addressed to A.R.

Competing financial interests

The authors declare no competing financial interests.